

Simulations of Spinodal Nucleation in Systems with Elastic Interactions

C. J. Gagne

Department of Physics, Clark University, Worcester, MA 01610

W. Klein,* T. Lookman, and A. Saxena

Theoretical Division, Los Alamos National Laboratory, Los Alamos, NM 87545

H. Gould

Department of Physics, Clark University, Worcester, MA 01610

(Dated: August 14, 2018)

Systems with long-range interactions quenched into a metastable state near the pseudospinodal exhibit nucleation that is qualitatively different than the classical nucleation observed near the coexistence curve. We have observed nucleation droplets in our Langevin simulations of a two-dimensional model of martensitic transformations and have determined that the structure of the nucleating droplet differs from the stable martensite structure. Our results, together with experimental measurements of the phonon dispersion curve, allow us to predict the nature of the droplet. These results have implications for nucleation in many solid-solid transitions and the structure of the final state.

PACS numbers: 64.60.Qb, 81.30.Kf, 05.10.-a, 05.70.Jk, 64.60.Fr

An outstanding challenge in the physics of solid-solid phase transformations is to understand the nucleation and growth of the transformed phase in strain based materials such as martensites, ferroelectrics, and multiferroics. Although ideas based on classical nucleation theory have been invoked to describe nucleation phenomena in these materials [1, 2, 3, 4, 5, 6], it is possible that the presence of long-range elastic forces substantially influences the probability of nucleation and subsequent growth that determines processing and material behavior. For example, the transformation susceptibility determined by nucleation is one of the basic factors for the hardenability of steels. Even though heterogeneous nucleation, which is sensitive to the distribution of appropriate structures in the parent phase from which product phase nuclei may be triggered, has long been considered important for martensites [7], homogeneous nucleation also has been observed if the transformational driving force is sufficiently large. However, due to the difficulty of experimentally determining nucleation droplet structure in martensites [1], very little is quantitatively known about the morphology of the nucleating droplet or “embryo,” including its size distribution or nucleation rate for homogeneous or heterogeneous nucleation. The aim of this work is to probe for the first time the nature of the nucleating droplet and associated fluctuations by performing mesoscale simulations using realistic nonlinear models for martensites. We find that the classical theory does not accurately describe the structure of the nucleating droplet, but that concepts associated with nucleation near a spinodal [8, 9] account for the observed

droplet morphology. In addition, our work provides the basis for investigating nucleation in systems where long-range elastic forces crucially determine the morphology.

Long-range elastic interactions are important in strain based materials, such as martensites, and result from the requirement of compatibility of strain components which is necessary to preserve the continuity of the elastic media [10, 11]. We refer to systems with long-range interactions as near-mean-field, and use several characteristics of mean-field theory to study nucleation in these systems. Mean-field systems have a well-defined spinodal, the limit of metastability; near-mean-field systems have a pseudospinodal, which becomes better defined as the range of interaction increases [12].

Spinodal nucleation, that is, nucleation close to the pseudospinodal, is predicted to produce a ramified droplet with a small amplitude [8, 9]. The droplet need not have the same structure as the stable phase [13, 14], unlike in classical nucleation where the droplet is compact and has the same structure as the stable phase [15]. Spinodal nucleation has been observed in molecular dynamic simulations of simple models [16, 17], but the concepts have never been tested on more realistic representations of materials such as martensites.

*Permanent Address: Department of Physics and Center for Computational Science, Boston University, Boston, MA 02215

We model a martensitic transformation using a Ginzburg-Landau (GL) free energy of the form [10, 11,

13]

$$F[\phi] = F_0 + F_{\text{grad}} + F_{\text{cs}} \quad (1a)$$

$$F_0 = \int_0^L d^2r [\tau\phi^2 - 2\phi^4 + \phi^6] \quad (1b)$$

$$F_{\text{grad}} = \int_0^L d^2r \left[\frac{a}{4}(\nabla\phi)^2 + \frac{b}{8}(\nabla^2\phi)^2 \right] \quad (1c)$$

$$F_{\text{cs}} = \int_0^L d^2r \left[\frac{A_1}{2}\epsilon_1^2 + \frac{A_2}{2}\epsilon_2^2 \right] \quad (1d)$$

$$\approx \int_0^L d^2r d^2r' U(\vec{r} - \vec{r}') e^{-|\vec{r} - \vec{r}'|/R} \phi(\vec{r}) \phi(\vec{r}'), \quad (1e)$$

where ϕ is the deviatoric strain, e_1 is the shear strain, e_2 is the compressional strain, $U(\vec{r} = \vec{r} - \vec{r}')$ is the Fourier transform of

$$\hat{U}(\vec{k}) = \frac{A_1}{2} \frac{(k_x^2 - k_y^2)^2}{\left[k^4 + 8\frac{A_1}{A_2} k_x^2 k_y^2 \right]}, \quad (2)$$

$\tau = (\theta - \theta_c)/(\theta_0 - \theta_c)$, θ is the dimensionless temperature, θ_c is the critical temperature where the $\phi = 0$ austenite minimum of F_0 disappears, θ_0 is the temperature where the three minima of F_0 are degenerate, and R is the range of the interaction. For metals R is quite large. The quantity F_{cs} can be written as nonlocal surface and bulk terms in $\phi(\vec{r})$ by using the St. Venant compatibility equations [10]. If the width of the interface of the droplet scales as the correlation length ξ , the surface term can be neglected for $\xi \gg R$ [13, 18]. The exponential cutoff has been added to $U(\vec{r})$ in F_{cs} to simulate defects. All of the variables are dimensionless and scaled, as described in detail below.

We use overdamped Langevin dynamics so the equation of motion for $\phi(\vec{r}, t)$ is

$$\frac{\partial\phi(\vec{r}, t)}{\partial t} = -\frac{\delta F[\phi(\vec{r}, t)]}{\delta\phi(\vec{r}, t)} + \zeta(\vec{r}, t), \quad (3)$$

where the Gaussian noise ζ is related to the dimensionless temperature θ by the fluctuation-dissipation relation,

$$\langle \zeta(\vec{r}, t) \zeta(\vec{r}', t') \rangle = 2\theta \delta^2(\vec{r} - \vec{r}') \delta(t - t'). \quad (4)$$

Several predictions have been made [13] about the critical droplet when the system is quenched to just above the spinodal temperature, τ_s , so that $\Delta\tau = \tau - \tau_s \ll 1$. In $d = 2$ the nucleation barrier is proportional to the Ginzburg parameter $G \approx \xi^2 \phi^2 / (\theta\chi) \approx \xi^2 \phi^2 / (\theta_c\chi) \gg 1$, where $\chi \approx 2/\Delta\tau$ is the susceptibility. Because $\phi \approx \sqrt{\Delta\tau/4} \ll 1$, the droplet is difficult to distinguish from the metastable background. For $a > 0$, $\xi \approx \sqrt{a/(4\Delta\tau)}$ and $\tau_s = 0$ [13], so $G \approx a\tau/(8\theta_c)$. If $a < 0$, $\xi \approx \sqrt{|a|/(2\Delta\tau)}$ and $\tau_s = |a|^2/(8b)$, so $G \approx |a|\Delta\tau/(4\theta_c)$. The droplet is predicted to be modulated at the largest (real) value of the wavenumber k_0 at which the structure function $S(k) \approx [\tau \pm |a|k^2/4 + bk^4/8 + \tilde{U}(k)]^{-1}$ diverges.

If $a > 0$, $k_0 = 0$ and the droplet is homogeneous, with $\phi(\vec{r})$ in the droplet either everywhere positive or negative. If $a < 0$, $k_0 = \sqrt{|a|/b}$, and the droplet is modulated with wavelength $w = 2\pi\sqrt{b/|a|} \ll \xi$, with alternating regions of positive and negative $\phi(\vec{r})$.

One of our main goals is to simulate martensites as realistically as possible. To this end, we need to relate the dimensionless simulation parameters in Eq. (1) to empirically accessible parameters. By extending the potential [11] to include a second gradient term, the three-dimensional (elastic) free energy near the critical temperature in terms of measurable quantities is

$$F[\epsilon_3] = \int_0^L d^3r \left[\frac{C_1}{2}\epsilon_1^2 + \frac{C_2}{2}\epsilon_2^2 + \frac{C_3}{2}\epsilon_3^2 - \frac{C_4}{4}\epsilon_3^4 + \frac{C_6}{6}\epsilon_3^6 + \frac{\kappa_1}{2a_0^2}(\vec{\nabla}\epsilon_3)^2 + \frac{\kappa_2}{4a_0^4}(\nabla^2\epsilon_3)^2 \right], \quad (5)$$

where a_0 is the crystal lattice spacing, L is the linear dimension of the system, and C_1 through C_6 , κ_1/a_0^2 , and κ_2/a_0^4 are elastic constants in units of N/m². $L/a_0 \gg \xi$ to minimize finite size effects. All the parameters in Eq. (5) can be determined empirically [11]; for example, κ_1/a_0^2 is determined from the curvature at small k of the phonon dispersion curve obtained from neutron scattering experiments [19]. We scale all the elastic constants by $A_0 = 9C_4^3/(128C_6^2)$ and the strains by $\epsilon_0 = \sqrt{3C_4/(4C_6)}$ to make the two martensite minima of the homogeneous part of F in Eq. (1b) near unity, and we scale all distances by a_0 . We define the dimensionless variables $\vec{r} = \vec{r}/a_0$, $\tilde{L} = L/a_0$, $\tilde{F} = F/(A_0a_0^3)$, $e_{1,2} = \epsilon_{1,2}/\epsilon_0$, $\phi = \epsilon_3/\epsilon_0$, $A_{1,2} = C_{1,2}\epsilon_0^2/A_0$, $\tau = C_3\epsilon_0^2/(2A_0)$, $a = 2\kappa_1\epsilon_0^2/(A_0a_0^2)$, and $b = 2\kappa_2\epsilon_0^2/(A_0a_0^4)$.

To find the proper scaling for the time, noise, and the temperature, we use the Langevin equation for $\epsilon_3(\vec{r}, t)$, which is Eq. (3) with $\phi \rightarrow \epsilon_3$, $F[\phi] \rightarrow F[\epsilon_3]$, and an explicit friction coefficient γ multiplying the time derivative. The dimensionless time and noise are $\tilde{t} = A_0a_0t/(L\gamma\epsilon_0^2)$ and $\tilde{\zeta} = L\epsilon_0\zeta/(A_0a_0)$. The factor of L is a result of going from $\epsilon_3(x, y, z, t)$ to $\phi(x, y, t)$. The fluctuation-dissipation relation Eq. (4) requires that we define $\theta = k_B T/(A_0a_0^3)$. θ_c and θ_0 are defined similarly with T replaced by T_c , the critical temperature, and T_0 is the temperature at which the three minima of the homogeneous part of F in Eq. (5) are degenerate. Note that we can change the effective temperature of the simulations either by changing T or a_0 . We drop all tildes in the following.

To discretize the Langevin equation, we used a simple forward Euler method [20] for the time derivative. Higher order algorithms take more time and give similar results. The random noise ζ is computed by multiplying the standard deviation of the noise σ_ζ by a random number chosen from a Gaussian distribution with unit variance, $G_{i,j,\alpha}$ [20]. On the lattice $\delta^2(\vec{r} - \vec{r}') \approx 1/\delta x^2$ and $\delta(t - t') \approx 1/\delta t$, so $\zeta(\vec{r}, t) \approx \sigma_\zeta G_{i,j,\alpha}$, where $\sigma_\zeta = \sqrt{2\theta/(\delta x^2 \delta t)}$. The treatment of the spatial derivatives and the nonlocal term is not as simple, however.

The nonlocal term in the Langevin equation that arises from Eq. (1e) is a convolution with the kernel $\hat{K}(\vec{k}) = \int d^2\rho U(\vec{\rho})e^{-|\vec{\rho}|/R}e^{-i\vec{k}\cdot\vec{\rho}}$. Here $\hat{K}(\vec{k})$ needs to be computed only once. The exponential factor $e^{-|\vec{\rho}|/R}$ is computed with the origin chosen at the center of the lattice so that it obeys periodic boundary conditions. On the discrete lattice the indices i and j correspond to x and y , l and m correspond to k_x and k_y , and α corresponds to t . We write $\phi(x, y, t) \rightarrow \phi_{i,j,\alpha}$, $\hat{U}(k_x, k_y) \rightarrow \hat{U}_{l,m}$, $e^{-|\vec{\rho}|/R} \rightarrow E_{i,j}$, and $\hat{K}(k_x, k_y) \rightarrow \hat{K}_{l,m} \approx \mathcal{F}[E_{i,j}\mathcal{F}^{-1}(\hat{U}_{l,m})]$, where \mathcal{F} and \mathcal{F}^{-1} represent fast Fourier transforms. The convolution integral is computed as:

$$\int_0^L d^2r' U(\vec{\rho})e^{-|\vec{\rho}|/R}\phi(\vec{r}', t) \approx \mathcal{F}^{-1}[\mathcal{F}(\phi_{i,j,\alpha})\hat{K}_{l,m}]. \quad (6)$$

The accuracy of our algorithm depends on treating both spatial derivatives to fourth order in δx , taking care to include cross terms in $\nabla^4\phi$. If we define $\oplus_{i,j}^{(1)} = \phi_{i+1,j} + \phi_{i-1,j} + \phi_{i,j+1} + \phi_{i,j-1}$, $\oplus_{i,j}^{(2)} = \phi_{i+2,j} + \phi_{i,j+2} + \phi_{i-2,j} + \phi_{i,j-2}$, and $\otimes_{i,j} = \phi_{i+1,j+1} + \phi_{i+1,j-1} + \phi_{i-1,j+1} + \phi_{i-1,j-1}$, then

$$\nabla^2\phi_{i,j} \approx \frac{1}{12(\delta x)^2}[-\oplus_{i,j}^{(2)} + 16\oplus_{i,j}^{(1)} - 60\phi_{i,j}] \quad (7a)$$

$$\nabla^4\phi_{i,j} \approx \frac{1}{(\delta x)^4}[\oplus_{i,j}^{(2)} - 8\oplus_{i,j}^{(1)} + 2\otimes_{i,j} + 20\phi_{i,j}]. \quad (7b)$$

We use the values $T_c = 268$ K, $T_0 = 290$ K, and $A_2 = 2A_1$ for all our simulations; these values correspond to FePd [11] so that our simulations are as realistic as possible. We also used $L = 64$ and $\delta x = 0.5$. Our procedure is to fix δx and $\delta t = 0.01$ and choose the values of the gradient parameters a and b so that the numerical solution is stable. Our numerical solutions were checked for accuracy by comparing the simulation results to the exact analytical solution for the linear case without the noise and nonlocal terms. Numerical stability for the complete equation of motion was checked by varying δt and δx . We limit ourselves to a and b such that the Ginzburg parameter $G \approx 5$ and $\xi \approx 16 = L/4$. We choose $A_1 < 1$ so that the core of the droplet will be more visible. We varied the nucleation rate primarily by changing a_0 .

For $a > 0$ we take $a = 6.32$, $b = 0.01$, $R = 6.4$, $\tau = 6.17 \times 10^{-3}$, $A_1 = 1 \times 10^{-3}$, and $a_0 = 2.1544 \times 10^{-8}$ m. FePd has a crystal lattice spacing of ≈ 3 Å, so this value of a_0 corresponds to a coarse-graining factor of 70 and sample size of about 1.38 μm. The value of τ corresponds to $T = 268.14$ K, and a corresponds to $\kappa_1/a_0^2 = 2.79 \times 10^9$ N/m². The value of a is reasonable compared to the value of 2.5×10^{10} N/m² for FePd quoted in Ref. [11].

For $a < 0$ we take $a = -1.61$, $b = 0.652$, $R = 4$, $\tau = 0.5$, $A_1 = 0.6$, and $a_0 = 2.7 \times 10^{-8}$ m. These values correspond to the modulation wavelength $w \approx 4$, $\tau_s = 0.49695$, $T = 279$ K, and $\Delta\tau = 3.048 \times 10^{-3}$.

We begin the simulation with $\phi(\vec{r})$ chosen at random around the metastable austenite minimum at $\phi = 0$.

Within a short time, $\phi(\vec{r})$ equilibrates at the chosen temperature. On a time scale much longer than the initial equilibration, the thermal noise causes a critical droplet to appear. By looking at the evolution of the spatial average, $\langle\phi^2(t)\rangle$, we can make an estimate of the nucleation time. From Fig. 1 we see that the system went from a metastable state with $\langle\phi^2\rangle \sim 0$ to the stable state with $\langle\phi^2\rangle \sim 1$ at the time $t = 2430$. Because we expect the amplitude of the droplet to be close to that of the metastable phase, we expect the nucleation time to be before the rapid increase in $\langle\phi^2\rangle$.

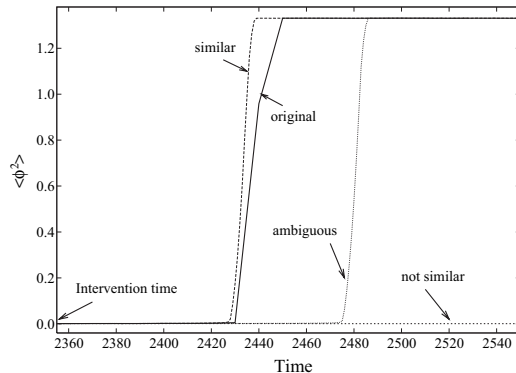


FIG. 1: Evolution of $\langle\phi^2(t)\rangle$ for $a > 0$; the original run and three interventions at $t = 2355$. $\langle\phi^2(t)\rangle$ of the original run grows rapidly from its metastable value to the stable value at $t \approx 2430$. If the intervention run is similar to the original run, the same droplet is assumed to have grown; otherwise, it is assumed that the same droplet did not grow. Some interventions are ambiguous. In this run the intervention time of 2355 is close to the estimated nucleation time of $t_n^+ = 2356 \pm 35$.

To determine the nucleation time more precisely, we use an intervention technique [21]. Because the nucleation droplet is a saddle point [8, 21], the droplet has an equal probability of growing to the stable state or shrinking back to the metastable state if we perturb the system at the nucleation time. We can use this saddle point property to help us find the nucleation time. We restart the simulation at the estimated nucleation time, and integrate the equations of motion using a new sequence of random numbers for the thermal noise. Our criterion is that if 8 ± 4 of the 16 runs with different random number sequences show that $\langle\phi^2\rangle$ grows at roughly the same time as in the original run, then the intervention time is equal to the nucleation time. We can then look at snapshots of $\phi(x, y)$ to see if we can identify the droplet.

For $a > 0$, the nucleation time is $t_n^+ = 2356 \pm 35$, corresponding to Fig. 1. A snapshot of $\phi(x, y)$ at $t = 2356$ is shown in Fig. 2a. Even though only the core of the droplet is visible above the noise, we can see that the droplet is homogeneous, as predicted.

For $a < 0$, the nucleation time is estimated to be $t_n^- = 1236.5 \pm 1.5$. The error in the nucleation time is much less than for $a > 0$ because the slower growth in $\langle\phi^2\rangle$ for $a < 0$ makes fewer of the interventions ambiguous. A

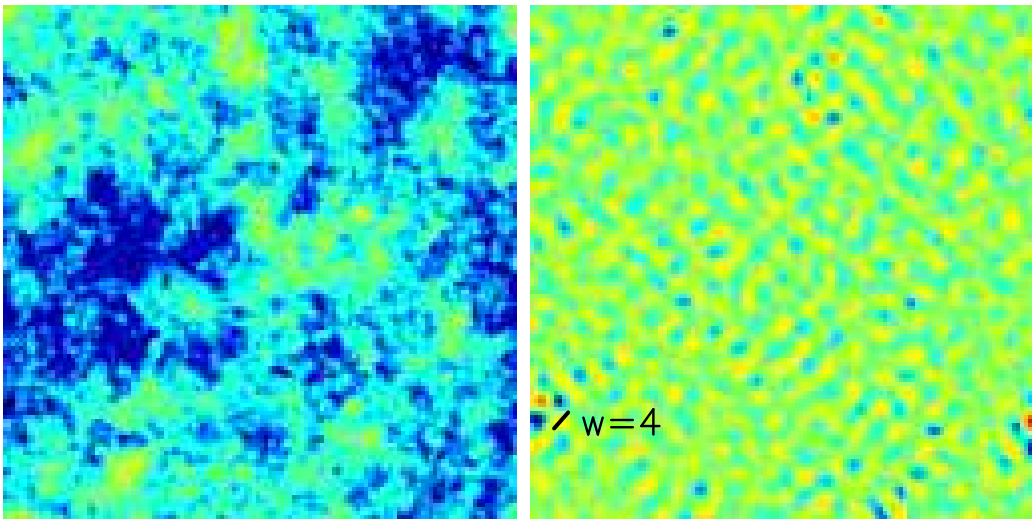


FIG. 2: (Color) From left: (a) The deviatoric strain $\phi(x, y)$ for $a > 0$ at the estimated nucleation time $t_n^+ = 2356$. The amplitude of ϕ ranges from -0.08 (dark blue) to 0.025 (yellow). The part of the droplet visible above the noise is clearly homogeneous, showing no modulations between the two low temperature minima (red and blue). (b) The deviatoric strain $\phi(x, y)$ for $a < 0$ at the estimated nucleation time $t_n^- = 1236.5$. The amplitude of ϕ ranges from -0.2 (dark blue) to 0.2 (red). In the part of the droplet that is visible, the modulations between the low temperature minima (red and blue) have the wavelength predicted by Ref. [13] to be $w \approx 4$.

snapshot of the field at $t = 1236.5$ is shown in Fig. 2b. As predicted in Ref. [13], the droplet has modulations with wavelength $w \approx 4$. This modulation is different from the twinning in the stable phase which occurs at wavelength $\lambda \sim \sqrt{L} = 8$ [10].

These results are important for nucleation in many functional materials with long-range interaction in which strain couples to some other physical variable, e.g. polarization (in ferroelectrics), magnetization (in magnetoelectrics), and other multiferroics. We found that in elastic systems the description of nucleation is subtle due to the presence of bulk/interface elastic compatibility constraints that are manifested as long-range interactions. In summary, when the austenite is quenched to near the pseudospinodal, the structure of the nucleation droplet is different than the structure of the stable martensite phase. If the curvature of the phonon dispersion curve at small k is positive, then $a > 0$ and the droplet is homogeneous.

If the curvature is negative, then $a < 0$ and the droplet is modulated with a wavelength w . The parameters we used are consistent with austenite to martensite transitions in FePd. We conclude, therefore that the classical nucleation picture is not applicable to these transitions and that the spinodal nucleation scenario is the better approach to understanding these transitions.

Acknowledgments

C.J.G. would like to thank Daniel Blair for his assistance with Fig. 2, and LANL where some of this work was done. W. K. acknowledges support from ASC Materials Modelling Program at LANL. Work at LANL was supported by the U.S. Department of Energy.

-
- [1] A. Borgenstam, *Mat. Sci. and Eng. A* **273**, 425 (1999).
 - [2] Z. Nishiyama, *Martensitic Phase Transformations* (Academic Press, New York, 1978).
 - [3] R. Oshima et al., *Metall. Trans. A* **19**, 803 (1988).
 - [4] G. B. Olson and A. L. Roitburd, Chap. 9 of *Martensite*, ASM International, G. B. Olson and W. S. Owen, eds. (1992).
 - [5] A. C. E. Reid, G. B. Olson, and B. Moran, *Phase Transitions* **69**, 309 (1999).
 - [6] B. P. Van Zyl and R. J. Gooding, *Metall. Trans. A* **27**, 1203 (1996).
 - [7] G. B. Olson and M. Cohen, *Met. Trans. A* **7**, 1897 (1976).
 - [8] C. Unger and W. Klein, *Phys. Rev. B* **29**, 2698 (1984).
 - [9] W. Klein and F. Leyvraz, *Phys. Rev. Lett.* **57**, 2845 (1986).
 - [10] T. Lookman et al., *Phys. Rev. B* **67**, 024114 (2003), S. R. Shenoy et al., *Phys. Rev. B* **60**, R12537 (1999).
 - [11] S. Kartha et al., *Phys. Rev. B* **52**, 803 (1995).
 - [12] D. W. Heermann et al., *Phys. Rev. Lett.* **49**, 1262 (1982).
 - [13] W. Klein et al., *Phys. Rev. Lett.* **88**, 085701 (2002).
 - [14] W. Klein, *Phys. Rev. E* **64**, 056110 (2001).
 - [15] J. S. Langer, *Ann. Phys.* **41**, 108 (1967).
 - [16] J. Yang et al., *J. Chem Phys.* **93**, 711 (1990)
 - [17] F. J. Cherne et al., cond-mat/0302491.

- [18] C. J. Gagne et al., in preparation.
- [19] M. Sato et al., J. Physics F: Met. Phys. **12**, 2117-2129 (1982)
- [20] W. H. Press et al., *Numerical Recipes in FORTRAN: The Art of Scientific Computing*, 2nd ed. (Cambridge University Press, Cambridge, 1992).
- [21] L. Monette and W. Klein, Phys. Rev. Lett. **68**, 2336 (1992).